FAST'93

Surface Piercing Propellers –Propeller/Hull Interaction

1. INTRODUCTION

The use of surface piercing propellers has become common place in many types of high speed craft. The applications have evolved from racing and pleasure craft to recent patrol and commercial craft. As a result of both prototype trials and tests at model scale it has been observed that the magnitude of propeller vertical and side forces as well as propeller bending moments can have a significant influence on vessel performance and shaft stresses. For the vessel designer little systematic data for the calculation of these so-called secondary propeller forces seems to be available and estimates are usually of pure empirical nature.

It is the purpose of this paper to present secondary force coefficients obtained from model tests with a series of four-bladed surface piercing propellers referred to as *Rolla Propeller Series* (ROSE and KRUPPA 1991). Vessel designers can use this data to estimate propeller vertical and side forces and to understand the influence of propeller dimensions and the effects of propeller position. The data can also serve as a guide for optimizing vessel performance. Finally, the data permits to calculate shaft stresses in an adequate way by proper assessment of the maximum bending moment.

2. MODEL TESTS

For details of the five model propellers (P/D = 0.9, 1.1, 1.2, 1.4, 1.6), the test set-up, the test parameters and procedures it is referred to the paper by ROSE and KRUPPA (1991). The model propellers were tested in the free-surface cavitation tunnel K27 of the *Institut für Schiffs- und Meerestechnik* of *Technische Universität Berlin* behind a flat plate. Three combinations of shaft inclination and immersion ratio were investigated (4 deg. at 30 %, 8 deg. at 47 %, 12 deg. at 58 %). The paper presents design charts (J and η) for a moderate cavitation number (σ = 0.5) and vertical force ratios (F_V/T) for a low cavitation number (σ = 0.2), in both cases as a function of the propeller loading in terms of K_Q/J^5.Information on the thrust loading capacity (J and η versus K_T/J^2) is given for a high cavitation number (σ_{atm}).

The six-component propeller dynamometer used in the model test series permits to measure the forces F_a, F_x, F_y, the torque Q and the propeller bending moments M_x, M_y. Orientation of these quantities can be seen from Fig. 1. All model propellers of the series are right-handed. It is clearly distinguished between the axial shaft force F_a and the thrust T. The latter and the vertical force F_v are derived from

$$T = F_a \cos\alpha - F_x \sin\alpha$$

and

$$F_v = F_a \sin\alpha + F_x \cos\alpha \ .$$

3. RESULTS

3.1 Design Charts

For a low cavitation number ($\sigma = 0.2$) design charts are presented in Fig. 2...4, for the three geometric configurations investigated. The data points represent a random selection from the test results, taking usually every fourth of the total measuring points stored on disc.

For a given value of

$$K_Q / J^5 = \frac{P_d\, n^2}{2\pi\rho V^5} \qquad (1)$$

advance coefficient (J) and efficiency (η) can be determined for various pitch-diameter ratios. This in turn permits to derive the optimum propeller diameter (D = V/nJ). The propeller thrust can be calculated from

$$T = \eta \frac{2\pi\rho V^4}{n^2} (K_Q / J^5) \ . \qquad (2)$$

3.2 Secondary Propeller Force Ratios

For documentation of the secondary propeller forces and bending moments the following non-dimensional quantities are defined

vertical force ratio $$\frac{F_v}{T} = \frac{F_a \sin\alpha + F_x \cos\alpha}{F_a \cos\alpha - F_x \sin\alpha}$$

side force ratio $$\frac{F_s}{T} = \frac{F_y}{F_a \cos\alpha - F_x \sin\alpha}$$

bending moment ratio (about x-axis) $$\frac{M_x}{RT} = \frac{M_x}{R(F_a \cos\alpha - F_x \sin\alpha)}$$

bending moment ratio (about y-axis) $$\frac{M_y}{RT} = \frac{M_y}{R(F_a \cos\alpha - F_x \sin\alpha)} \ ,$$

where R is the propeller radius (D/2).

Using the propeller thrust to arrive at non-dimensional force ratios seems to be justifiable on the ground that the thrust should be a known quantity related to the expected vehicle drag. If the bending moments had been normalized with the propeller radius (R) and the axial force of the propeller (F_a) the bending moment ratios would have determined the non-dimensional x- and y-coordinates (see Fig. 1) of the axial force excentricity. Using the propeller thrust (T) instead seems again justifiable, as the thrust (or true propulsion force) is more readily available. Where noticeable differences between thrust and axial force occur, as is the case for large shaft angles, the bending moment ratios as defined above should not be interpreted as "thrust" excentricity.

Force and bending moment ratios for a small cavitation number (σ = 0.2) are presented for the three different combinations of immersion ratio and shaft angle (30 % at 4 deg., 47 % at 8 deg., 58 % at 12 deg.) in Fig. 5.....16, again on the basis of propeller loading in terms of K_Q/J^5. As can be seen, the force and moment ratios converge at high propeller loading and become more or less independent of pitch-diameter ratio. At low propeller loading, where the thrust reaches very low values, the data become more dependent on pitch-diameter ratio, not necessarily in a uniform way. Apparent anomalies have repeatedly been checked, in some cases by re-testing after two years, but were found to recur. As an exception, results of M_y/RT are not available for the mean shaft angle and P/D = 0.9 (Fig. 15).

4. PROPELLER/HULL INTERACTION

4.1 Bearing Forces

In addition to thrust and torque, vertical and side forces are acting on a hull propelled by surface piercing propellers. In case of the *Rolla Propeller Series* the vertical forces are always directed upwards (Fig. 5.....7), thus tending to reduce the trim of the vehicle. This is in line with experience as far as propellers with little or no rake are concerned. Vertical forces reach their highest values when shaft inclination is large. Side forces, on the other hand, are largest when the immersion ratio is small. For very low immersion ratios and high pitch-diameter ratios the side force can be related to the torque of the propeller and expressed in the form

$$\frac{F_s}{T} = \chi \frac{J}{\pi\eta},$$

where $1.0 \leq \chi \leq 1.2$ has been found in numerous experiments.

Running surface piercing propellers at positive yaw angles, i.e. turning a right-handed propeller about the x-axis in a clockwise direction to portside (see Fig. 1), will increase the thrust and reduce the side force. This effect is pronounced at small immersion ratios, but the effective loss in pitch has to be adequately compensated. Unfortunately, with the existing test set-up at the *Institut für Schiffs- und Meerestechnik* no experiments with propellers at yaw can be performed.

Usually, surface piercing propellers are installed as handed pairs, thus eliminating the side force effect on the hull. However, the inflow into the propellers is invariably subject to more or less extensive deadrise angles (β). Assuming constant deadrise angles near the stern and a flow direction parallel to the buttocks, the cavitation tunnel test results can be used to estimate vertical and side forces in an x'-y'-z' coordinate system, rotated about the deadrise angle β, as follows

$$F_v' = F_s \sin\beta + F_v \cos\beta \tag{3}$$

and

$$F_s' = F_s \cos\beta - F_v \sin\beta \, . \tag{4}$$

The formulae are applicable for positive side forces in the coordinate system defined in Fig. 1, i.e. for outward turning starboard propellers. The side force $F_s = F_y$ will thus contribute to lift the stern, whereas it will have the opposite effect for inward turning screws ($F_y < 0$). The magnitude of this effect is demonstrated by the sample calculation given in the Appendix and obviously very significant (Table 2).

Using the model test results obtained behind a flat plate for secondary force prediction of hulls with noticeable deadrise introduces an element of positive, and therefore beneficial, yaw. In practice, this will not occur if the shafts are aligned with the longitudinal axis of the hull. Toe-out of shafts may therefore be a desirable design element for outward turning propellers, in hulls with significant deadrise.

4.2 Shaft Stresses

In the coordinate system defined in Fig. 1 the maximum bending moment in the unsupported length of tailshaft (z_0) is obtained from

$$M_{bmax} = \sqrt{(M_x + F_y z_0)^2 + (M_y - F_x z_0)^2}$$

$$= RT\sqrt{\left(\frac{M_x}{RT} + \frac{F_y}{T}\frac{z_0}{R}\right)^2 + \left(\frac{M_y}{RT} - \frac{F_x}{T}\frac{z_0}{R_0}\right)^2} \, . \tag{5}$$

Although the propeller normal force component F_x has been measured it is not presented in this paper. One has to refer to the results presented for the vertical force ratio F_v/T (see Fig. 5.....7) and use the following relation in Equ. 5

$$\frac{F_x}{T} = \frac{F_v}{T}\cos\alpha - \sin\alpha \, . \tag{6}$$

The maximum bending stress for solid shafts is calculated from

$$s_{bmax} = 32\frac{M_{bmax}}{\pi D^3} \, .$$

In addition, the shaft is subject to the torsional load Q, with a maximum shear stress of

$$\tau_{max} = 16\frac{Q}{\pi D^3} .$$

Since the effect of axial load due to thrust is small and can be neglected the "comparative stress" s_c, as defined by "theory of elasticity", is obtained from the relation

$$s_c = \sqrt{s_{bmax}^2 + 3\tau_{max}^2}$$

and a "comparative stress" ratio can be written as follows

$$\frac{s_c}{\tau_{max}} = \sqrt{(\frac{2M_{bmax}}{Q})^2 + 3} . \qquad (7)$$

For the example given in the Appendix the effect of bending stresses is demonstrated in Table 3, for an unsupported length of tailshaft of $0.2 < z_0/D < 0.3$. As can be seen, shaft dimensions are clearly dependent on the permissible "comparative stress" level which is largely determined by the maximum bending moment (Equ. 5).

5. CONCLUSIONS

The magnitude of the secondary propeller forces in surface piercing propellers requires detailed analysis of propeller bearing forces, both with regard to vertical and side forces. This is demonstrated by the sample calculations presented in the Appendix. Table 2 shows that even for moderate values of shaft angle (α = 8 deg.) and propeller immersion (h/D = 47 %) the vertical force ratio may vary in the range $0.63 \geq F_V'/T \geq 0.33$, depending on deadrise angle and direction of shaft rotation. The side force ratio shows even larger variations ($0.44 \geq F_s'/T \geq -0.59$). The vessel designer must have sufficient knowledge of the reaction of the craft to bearing forces of this magnitude.

For selecting proper shaft dimensions the combined load of bending and torsion must be taken into account. The values of the "comparative stress" ratio in Table 3 clearly reveal that bending stresses are of decisive influence.

6. ACKNOWLEDGEMENTS

The authors wish to thank PHILIP ROLLA of *Rolla SP Propellers SA*, Switzerland for his continued permission and support in publishing the results of this and continuing investigations. The authors believe that in this way the hydrodynamics of surface piercing propellers will become better understood in the marine community. This in turn will be beneficial for their application and success in high-speed craft.

7. REFERENCES

ROSE J.C. and KRUPPA C.F.L. (1991) Surface Piercing Propellers - Methodical Series Model Test Results. In: FAST'91 (edited by K.O. Holden et al.), volume 2, pages 1129-1147, Tapir Publishers, Trondheim.

APPENDIX

Sample Calculations

Table 1 Design Condition

delivered power at propeller	P_d [kW]	1045
engine rate of revolutions	n_E [min^{-1}]	2300
reduction gear ratio	GR [-]	1.5:1
propeller torque	Q [kNm]	6.51
ship and propeller advance speed	V [kn]	55.0
cavitation number	σ [-]	~0.2
unsupported length of tailshaft	z_0 [m]	0.33
propeller loading (Equ. 1)	K_Q/J^5 [-]	0.00585

Table 2 Bearing Forces

geometric configuration						
immersion ratio	h/D	[-]	30 %		47 %	58 %
shaft angle	α	[deg.]	4		8	12
from design charts (Fig. 2....4)						
pitach-diameter ratio	P/D	[-]	1.4	1.6	1.6	1.6
efficiency	η	[-]	0.645	0.625	0.645	0.605
advance coefficient	J	[-]	1.16	1.22	1.38	1.44
by calculation						
thrust (Equ. 2)	T	[kN]	23.82	23.09	23.82	22.35
diameter (D=V/nJ)	D	[m]	0.954	0.907	0.802	0.769
from charts for secondary forces						
vertical force ratio (Fig. 5....7)	F_V/T	[-]	0.18	0.27	0.51	0.77
side force ratio (Fig. 8....10)	F_S/T	[-]	0.58	0.67	0.44	0.06
test condition (behind flat plate)						
vertical force	F_V	[kN]	4.29	6.23	12.15	17.21
side force	F_S	[kN]	13.82	15.47	10.48	1.34
β = 20 deg. deadrise (outward turn.)						
vertical force (Equ. 3)	F_V'	[kN]	8.76	11.15	15.00	16.63
side force (Equ. 4)	F_S'	[kN]	11.52	12.41	5.69	-4.63
β = 20 deg. deadrise (inward turn.)						
vertical force (Equ. 3)	F_V'	[kN]	-0.70	0.56	7.83	15.71
side force (Equ. 4)	F_S'	[kN]	-14.45	-16.67	-14.00	-7.15

Table 3 Shaft Stresses

geometric configuration						
immersion ratio	h/D	[-]	30 %		47 %	58 %
shaft angle	α	[deg.]	4		8	12
pitch-diameter ratio	P/D	[-]	1.4	1.6	1.6	1.6
diameter of propeller	D	[m]	0.954	0.907	0.802	0.769
from charts for secondary forces						
bending moment ratio about x-axis (Fig. 11....13)	M_x/RT	[-]	0.22	0.10	0.14	0.36
bending moment ratio about y-axis (Fig. 14....16)	M_y/RT	[-]	0.62	0.68	0.48	0.27
from Table 2 and by calculation (Equ. 6)						
normal force ratio (x-axis)	F_x/T	[-]	0.11	0.20	0.37	0.54
side force ratio (y-axis)	$F_y/T = F_s/T$	[-]	0.58	0.67	0.44	0.06
by calculation (Equ. 5)						
maximum bending moment at z_0	M_{bmax}	[kNm]	9.38	8.32	5.08	3.91
by calculation (Equ. 7)						
"comparative stress" ratio	σ_c/τ_{max}	[-]	3.36	3.09	2.33	2.11

FIGURES

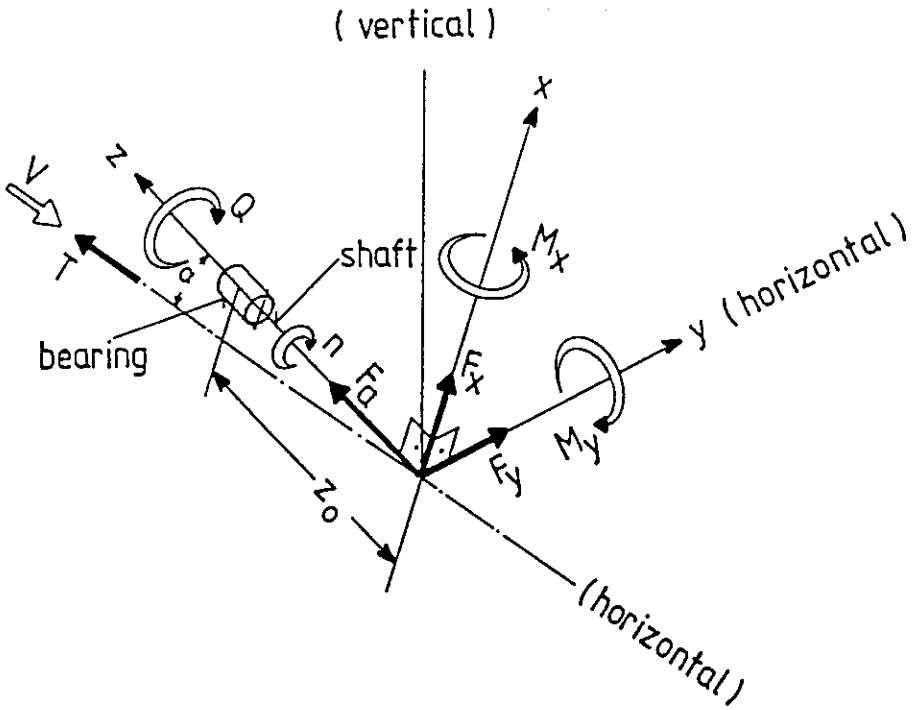

Fig. 1 Six-Component Propeller Forces

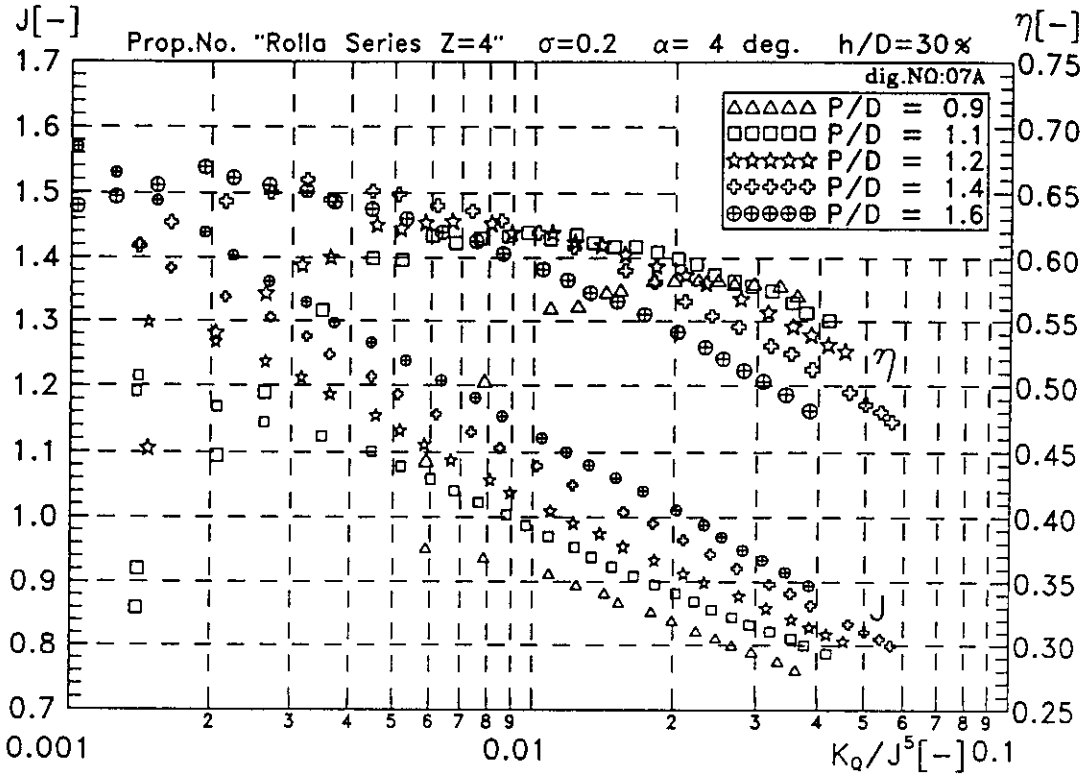

Fig. 2 Design Chart for Small Shaft Angle

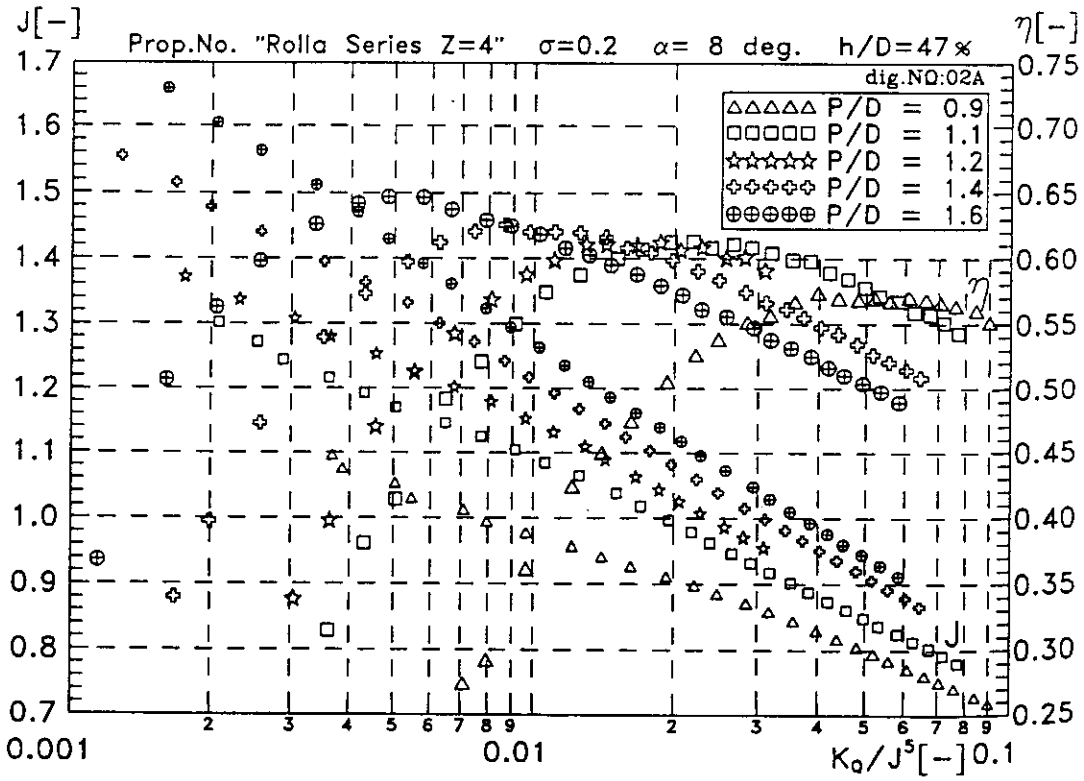

Fig. 3 Design Chart for Mean Shaft Angle

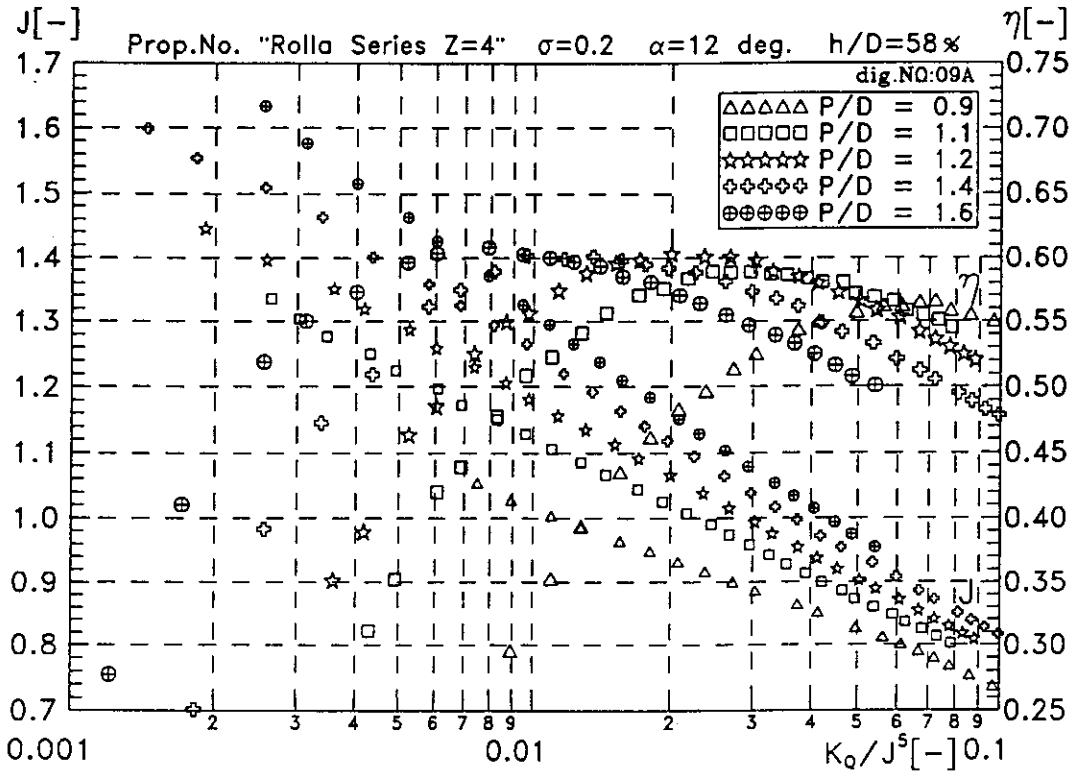

Fig. 4 Design Chart for Large Shaft Angle

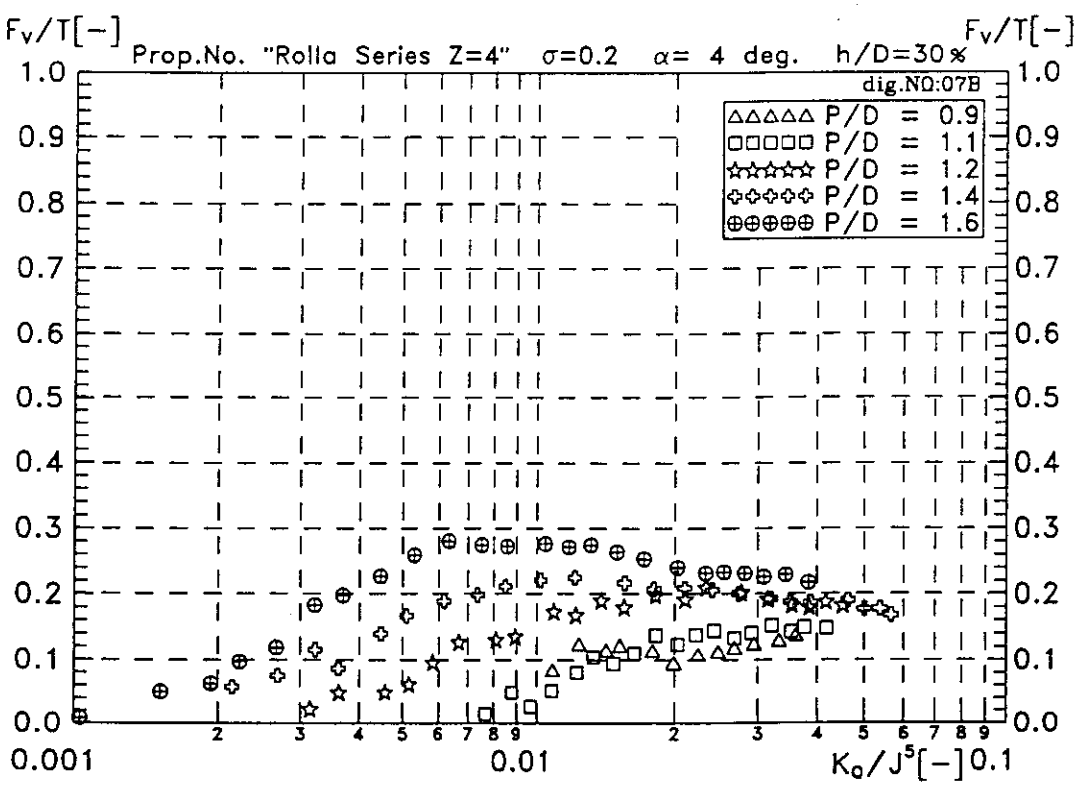

Fig. 5 Vertical Force Ratio for Small Shaft Angle

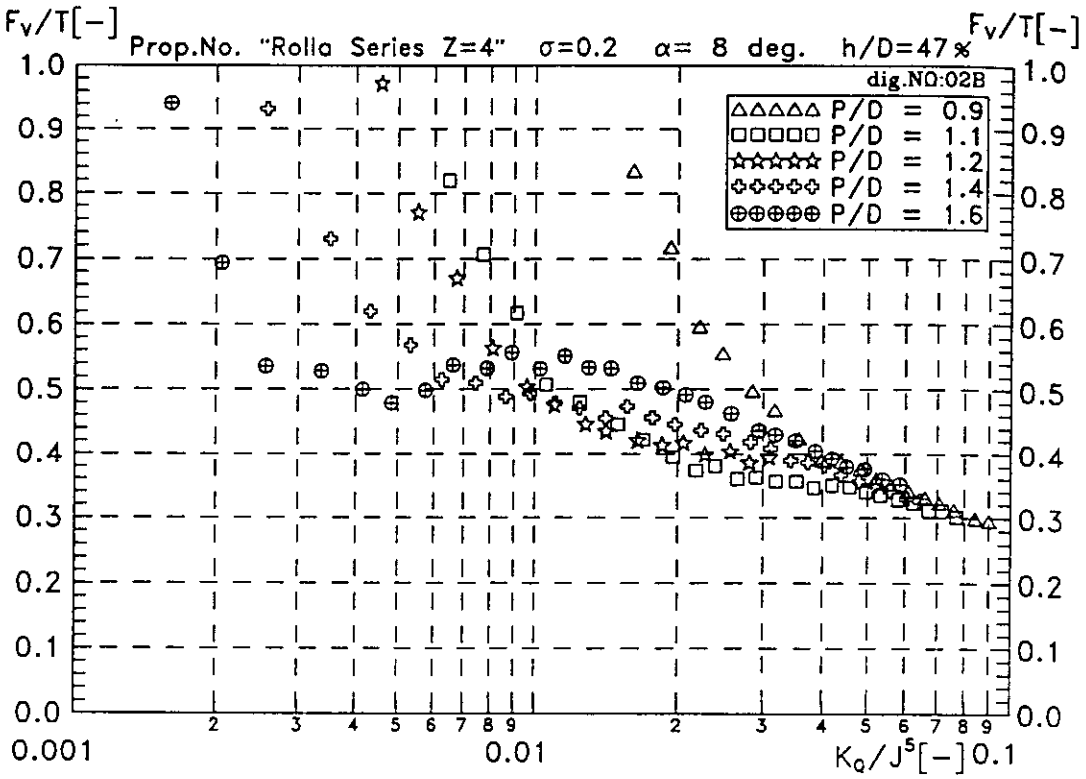

Fig. 6 Vertical Force Ratio for Mean Shaft Angle

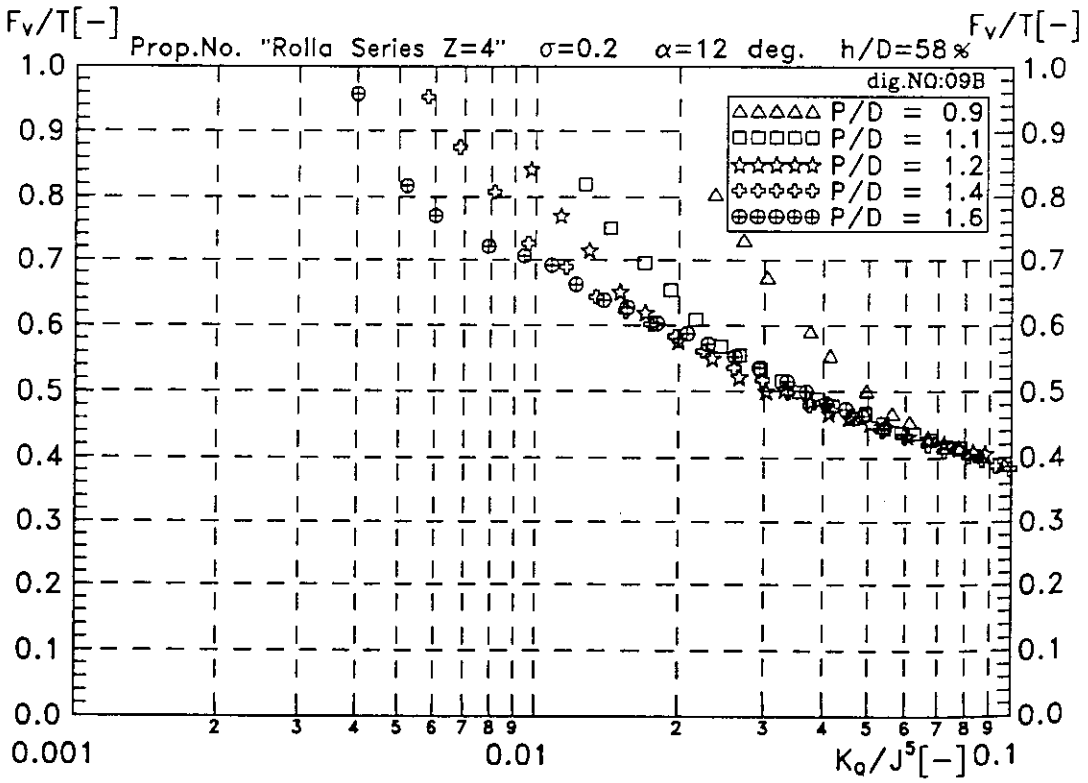

Fig. 7 Vertical Force Ratio for Large Shaft Angle

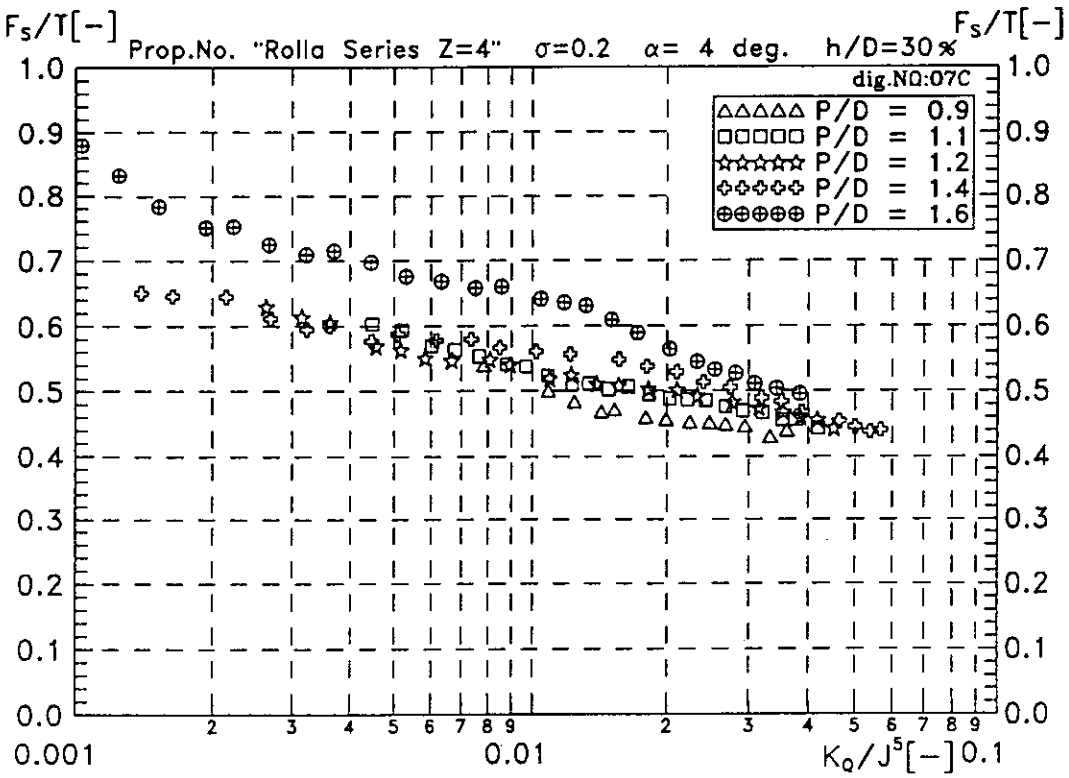

Fig. 8 Side Force Ratio for Small Shaft Angle

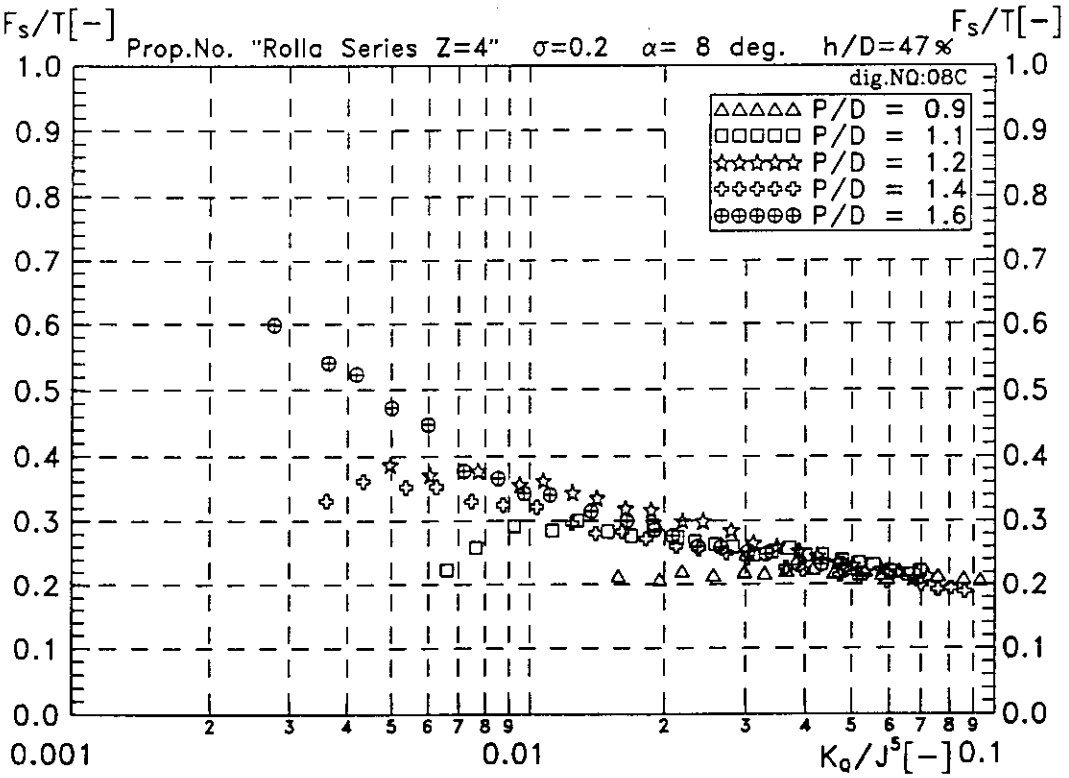

Fig. 9 Side Force Ratio for Mean Shaft Angle

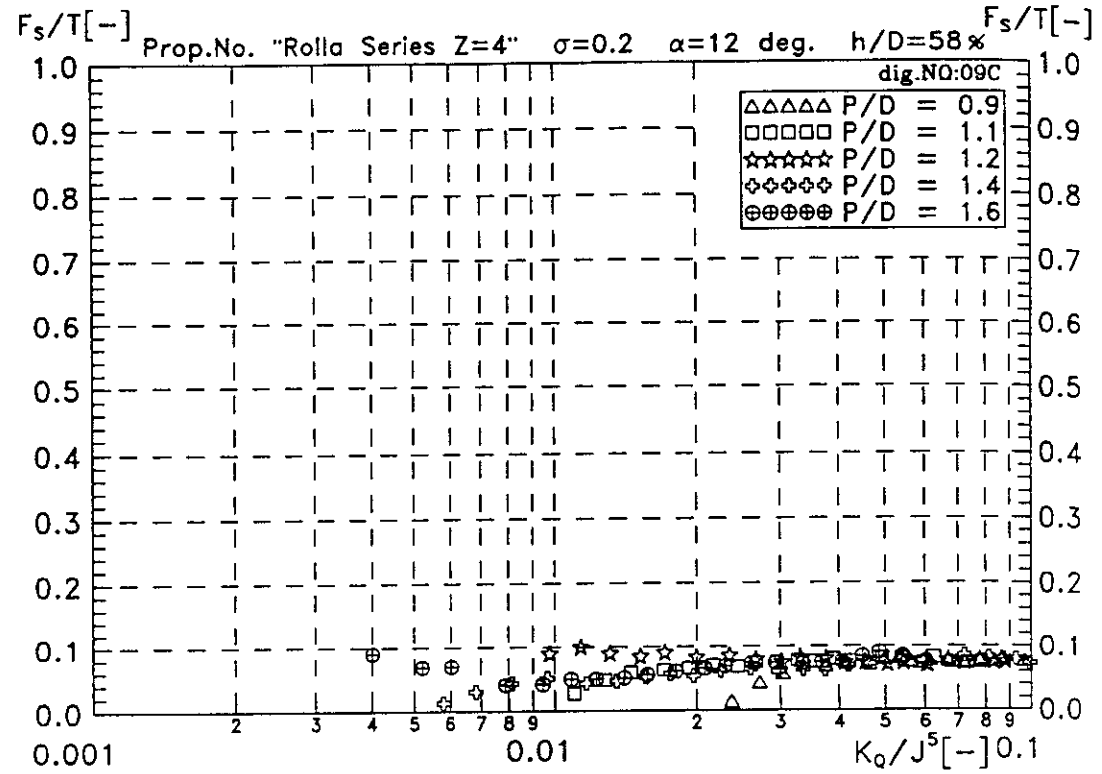

Fig. 10 Side Force Ratio for Large Shaft Angle

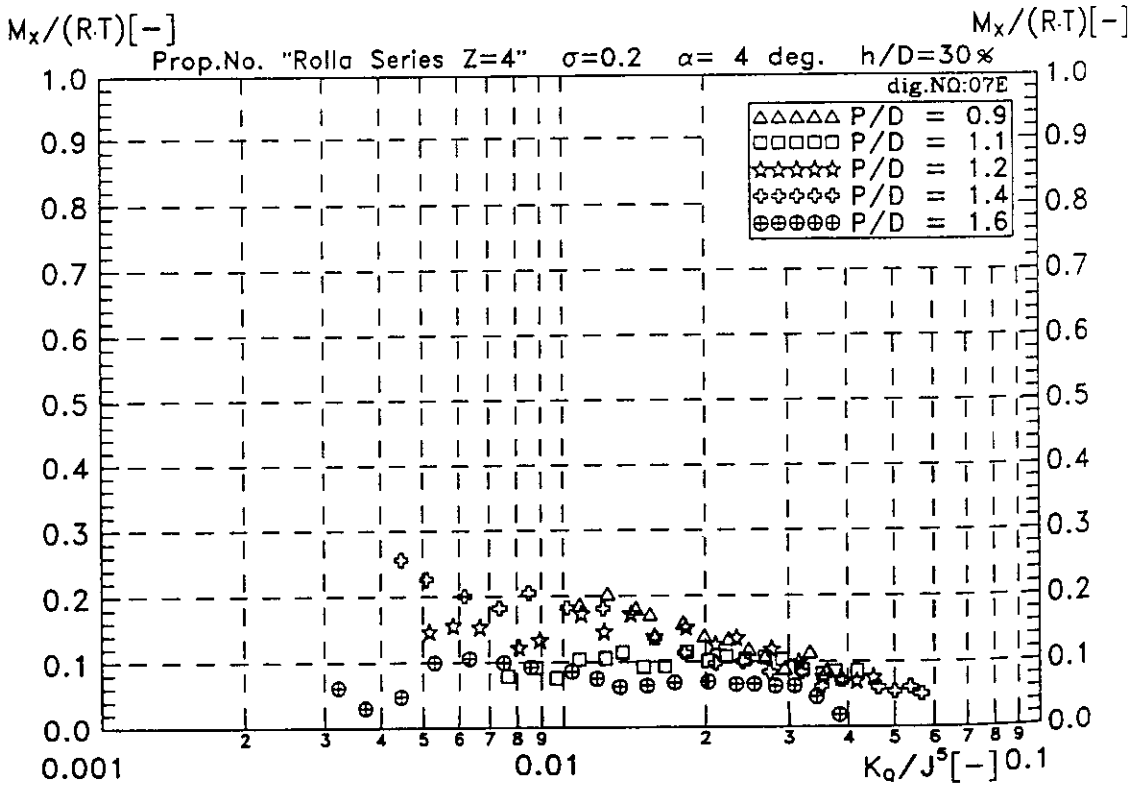

Fig. 11 Bending Moment Ratio about x-Axis for Small Shaft Angle

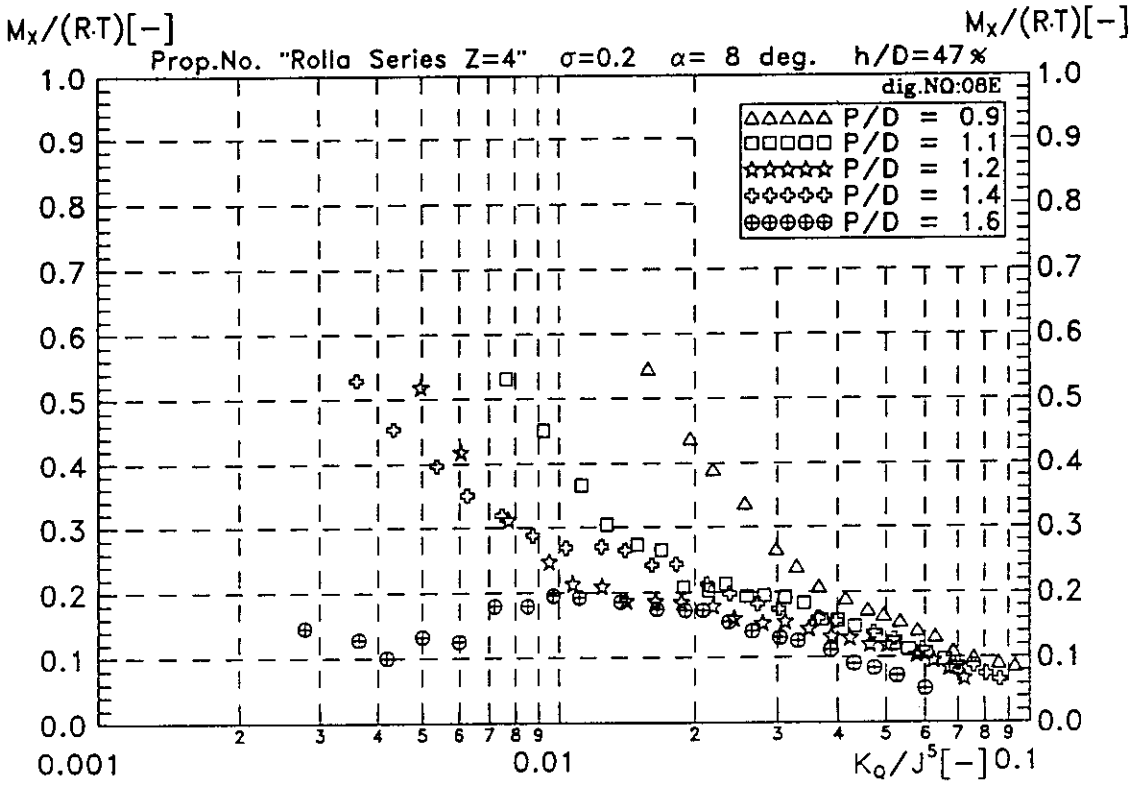

Fig. 12 Bending Moment Ratio about x-Axis for Mean Shaft Angle

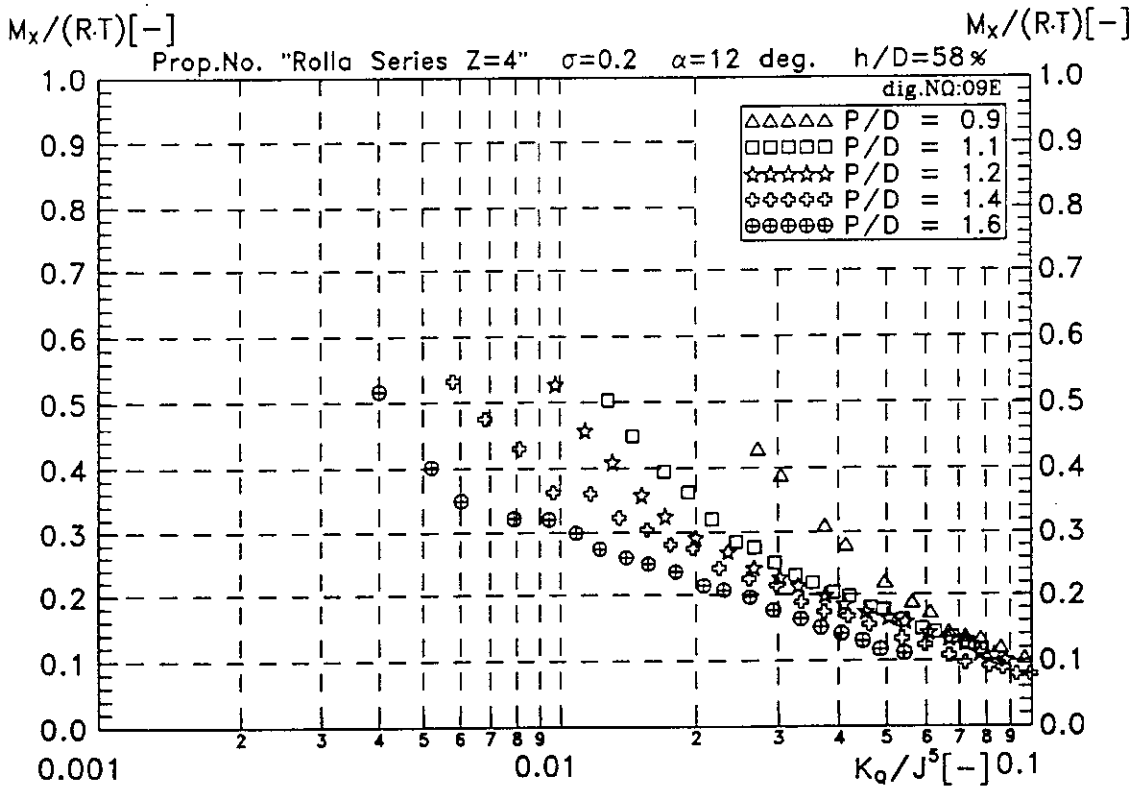

Fig. 13 Bending Moment Ratio about x-Axis for Large Shaft Angle

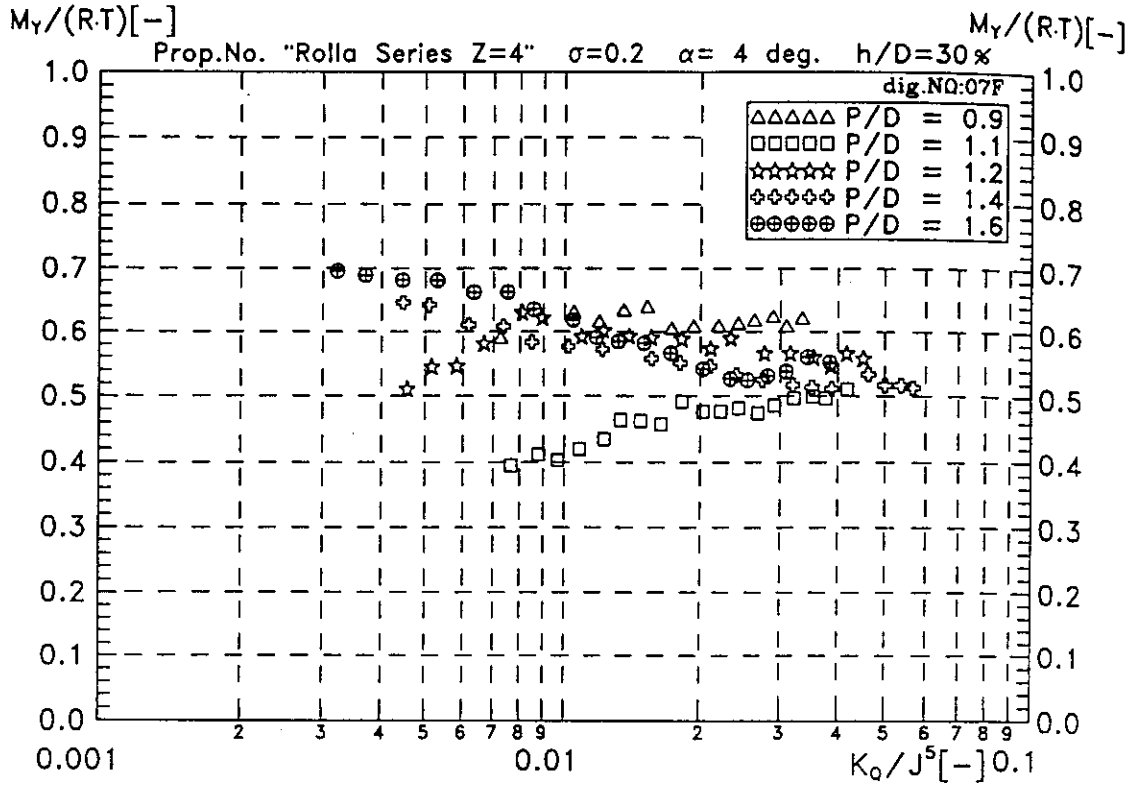

Fig. 14 Bending Moment Ratio about y-Axis for Small Shaft Angle

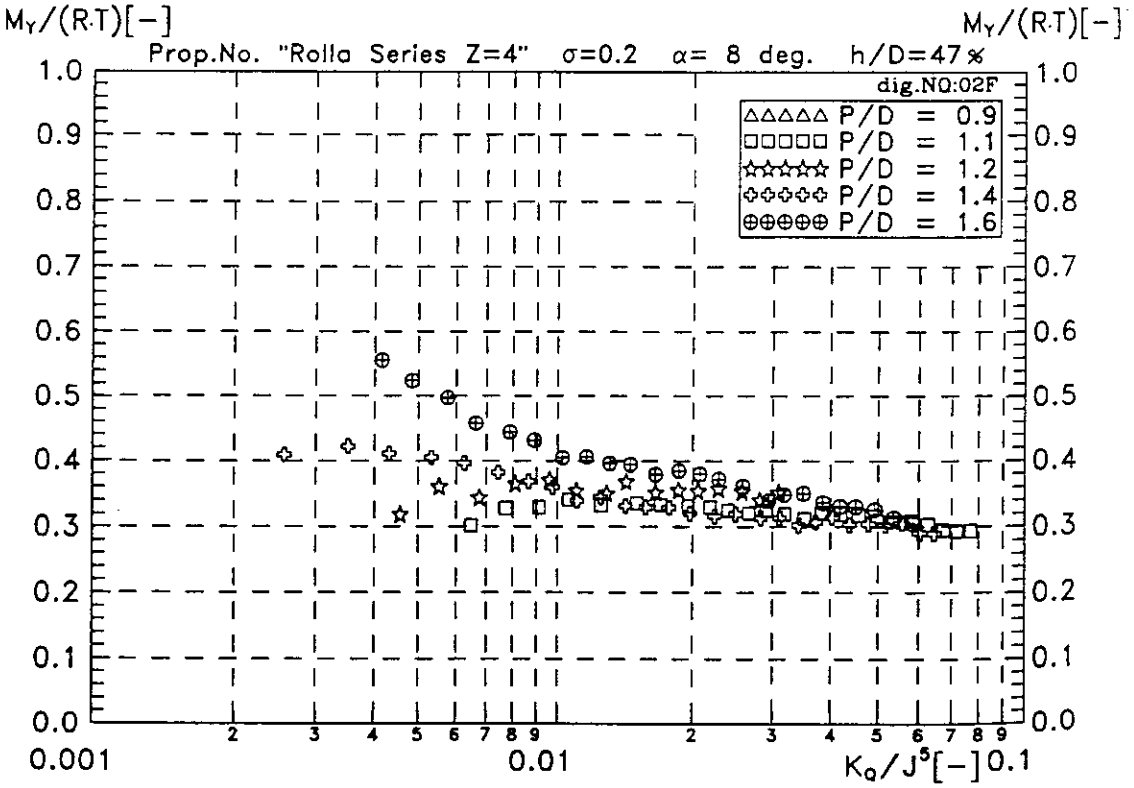

Fig. 15 Bending Moment Ratio about y-Axis for Mean Shaft Angle

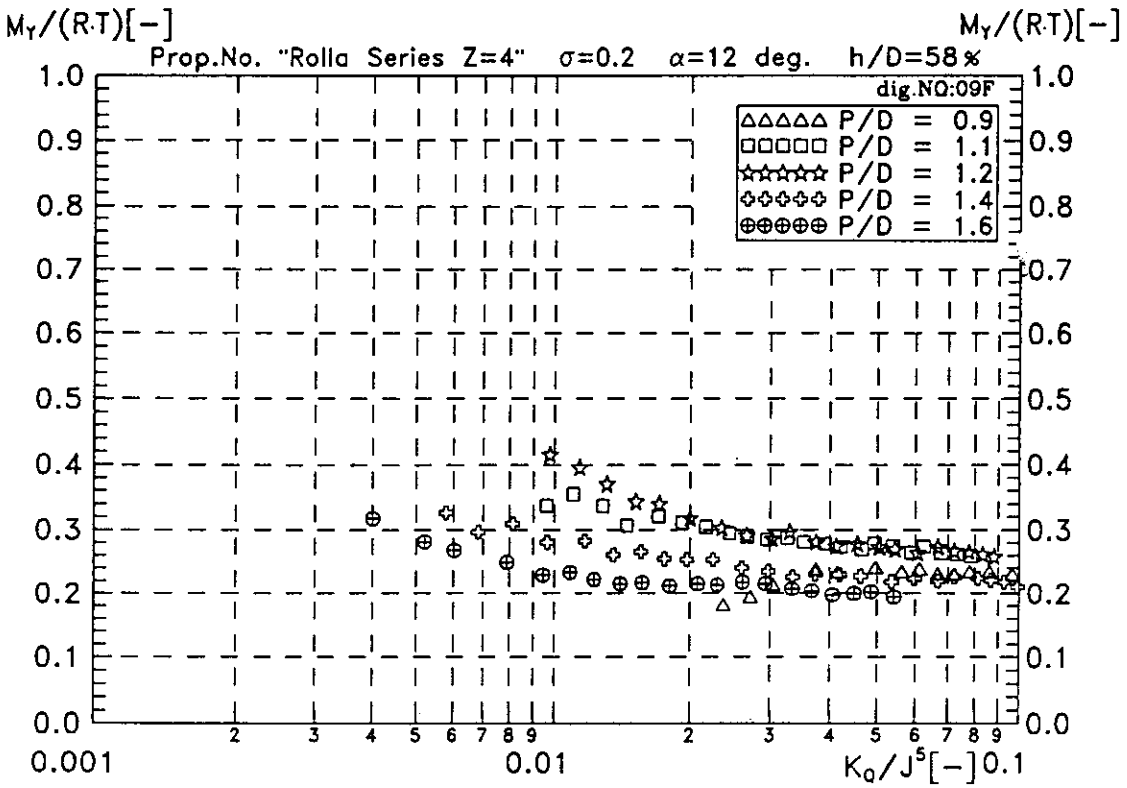

Fig. 16 Bending Moment Ratio about y-Axis for Large Shaft Angle